

A Simple CFD/CSD Loose Coupling Approach For Rotor Blade Aeroelasticity

Yasutada Tanabe, Shigeru Saito

Japan Aerospace Exploration Agency (JAXA)
7-44-1 Jindaiji Higashi-machi, Chofu, Tokyo, 182-8522, JAPAN
e-mail: tan@chofu.jaxa.jp

Key words: Rotorcraft, rotor blade, aeroelasticity, CFD/CSD coupling, overlapped grids

Abstract: An integrated fluid-structure coupled simulation code based on a loose coupling approach has been developed to investigate aeroelastic effects of helicopter rotor blades. Aerodynamic forces are obtained from an Euler solver in moving overlapped grids. The structural deformations are computed using the CFD-obtained aerodynamic forces by assuming periodicity of the aerodynamic forces and blade deformations for each rotor rotation. HART II data is used for the validation of the code. Test validation computation shows fast and stable convergences in trim adjustments, total thrust and moments and the elastic motions.

INTRODUCTION

Since helicopters are playing more important roles in human activities, for example, life saving and disaster relief, rescue directly on the highway, et al. The helicopter noise becomes a major concern when operating in the urban areas. There are more requirements for quieter helicopters. However, even current low noise helicopter designs have largely reduced the fly-over noise, the so called slap noise occurs when helicopter in descending flight still remains an annoying problem.

When helicopter is in descent flight, the generated blade tip vortices remain in the vicinity of the rotor plane which leads to strong interactions between the rotor blades and the tip vortices known as blade-vortex interaction (BVI). BVI also occurs during maneuvers at moderate advance ratios. BVI events cause impulsive changes in the airloads and thus impulsive shock wave like noise. These time-varying airloads affect rotor performance and also increase the structural fatigue as well. The strength of BVI is dependent upon several factors: miss distance, relative geometry of the blade and vortex, and the vortex core structure. The strength of a BVI decrease fast as the blade-vortex miss distance increase. Parallel BVI events are essentially two-dimensional in nature, and have strong transient characteristics. There are several researches on the parallel BVI by solving the two-dimensional Euler equations and have good comparison with experiments[1-4]. There is a parametric study on the parallel BVI by varying the miss distance and also the blade incidence by present authors [5].

A concentrated vortex core causes higher impulsive loading levels, and these higher levels are diminished for a diffused vortex core. Maintaining the size and strength of a vortex core is then important for capturing BVI with CFD methods. Euler and Navier-Stokes flow solvers capture the vortex core explicitly, but the vortex core is usually artificially diffused through under-resolution of the vortex core structure in the computational grid. The velocity profile along a radius from the vortex center, the vortex strength, and the size of the vortex core are correspondingly incorrect. The accuracy of the calculated transient blade surface pressure during BVI is then limited by the accuracy of the vortex structure. In a two-dimensional BVI computational study carried in a JAXA/ONERA cooperative research[6], it is found even with JAXA's 4th order spatial accurate

scheme, 15 points was required in the vortex radius to preserve the vortex strength nearly constant during long distance convection. Considering the experimental observed tip vortex core size of nearly 5% blade chord length, it seems quite impossible to realize such high resolution in a three-dimensional computation even for currently most advanced supercomputers to obtain a converged solution within reasonable time span.

Active controls of the blade have been proposed to reduce the BVI levels. Some intend to diffuse the tip vortex core through jet blowing or canard wing tips which usually accompany some performance penalties. The most currently pursued active control techniques are higher harmonic control (HHC) inputs applied at the blade root or by moving some small control surfaces on the blade (Active Flap, Active Tab, et al.) [7]. However, such higher harmonic controls could cause larger vibratory loads to the blade and their influences should be evaluated correctly during the design.

To balance all of the aerodynamic and inertial forces and moments, rotor blades undergo quite complicated motions. Because the blade generally has high aspect ratio, it is quite flexible in the flapping, torsional and lead-lag directions usually. During one rotor revolution, the blades can experience rapid changes in the applied loads and undergo substantial elastic deformations in response. There will be fatigue along with aeroelastic instability concerns. A comprehensive analytical tool is needed that can accurately model both the flow field around a rotor and the aeroelastic response of the rotor blades in the same process.

There are two ways to combine the fluid and structure dynamics analysis. They are called as loose (or weak) and tight (or strong) coupling. In the loose coupling approach, information is passed between CFD and CSD on a per blade period basis. In the tight coupling approach, the CFD and CSD codes are coupled at every time step and integrated simultaneously.

Altmikus [8] made comparisons with loose and tight coupling approaches using the CFD codes FLOWer and WAVES and the comprehensive code HOST. For high speed flight conditions, tight coupling achieved very similar results to loose coupling, but at 2.5 times the cost. Trim was also achieved quickly with the loose coupling approach.

Potsdam [9] used the OVERFLOW-D overset grid solver along with the comprehensive code CAMRAD-II to study various flight cases from the UH-60A Airloads Program flight test database. Potsdam also compared coupled CFD/CSD solutions with those just from comprehensive free wake analysis. Lim [10] used loose coupling between OVERFLOW-2 and CAMRAD-II for BVI airloads predictions for the UH-60A, the HART-I, and HART-II rotors. Hill [11] used OVERFLOW-2 coupled with RCAS to study the HART-II rotor. The results are quite similar to those of OVERFLOW-2/CAMRAD-II by Sim and Lim [12]. The BVI occurrence are captured quite well but the average of airloads $C_n M^2$ are significantly lower than experiments.

In JAXA, a low noise rotor blade with active flap is under development [13]. There are needs for the correct aeroelastic analysis for the blade with active controls and good prediction of the noise reduction effects. Both tight and loose CFD/CSD coupling methods are under studies in JAXA [14, 15]. Simple coupling approaches without using the comprehensive CSD code but integrating the CSD core code into existing CFD code are desired. In this paper, the loose coupling approach and its result are described.

1. NUMERICAL METHOD

1.1 CFD Code – JAXA_ov3d

The newly developed CFD code is referred as JAXA_ov3d. Governing equations for JAXA_ov3d are full unsteady Navier-Stokes equations. But for this test validation computation, considering the computational efficiency, only the Euler solver module is used. A moving overlapped grid approach [16] is used in JAXA_ov3d. The grid system used in this study is shown in figure 1. There are three layers of grids, the outer background grid, the inner background grid, and the inner moving blade grids. Total grid point number for this test study is about 10 millions.

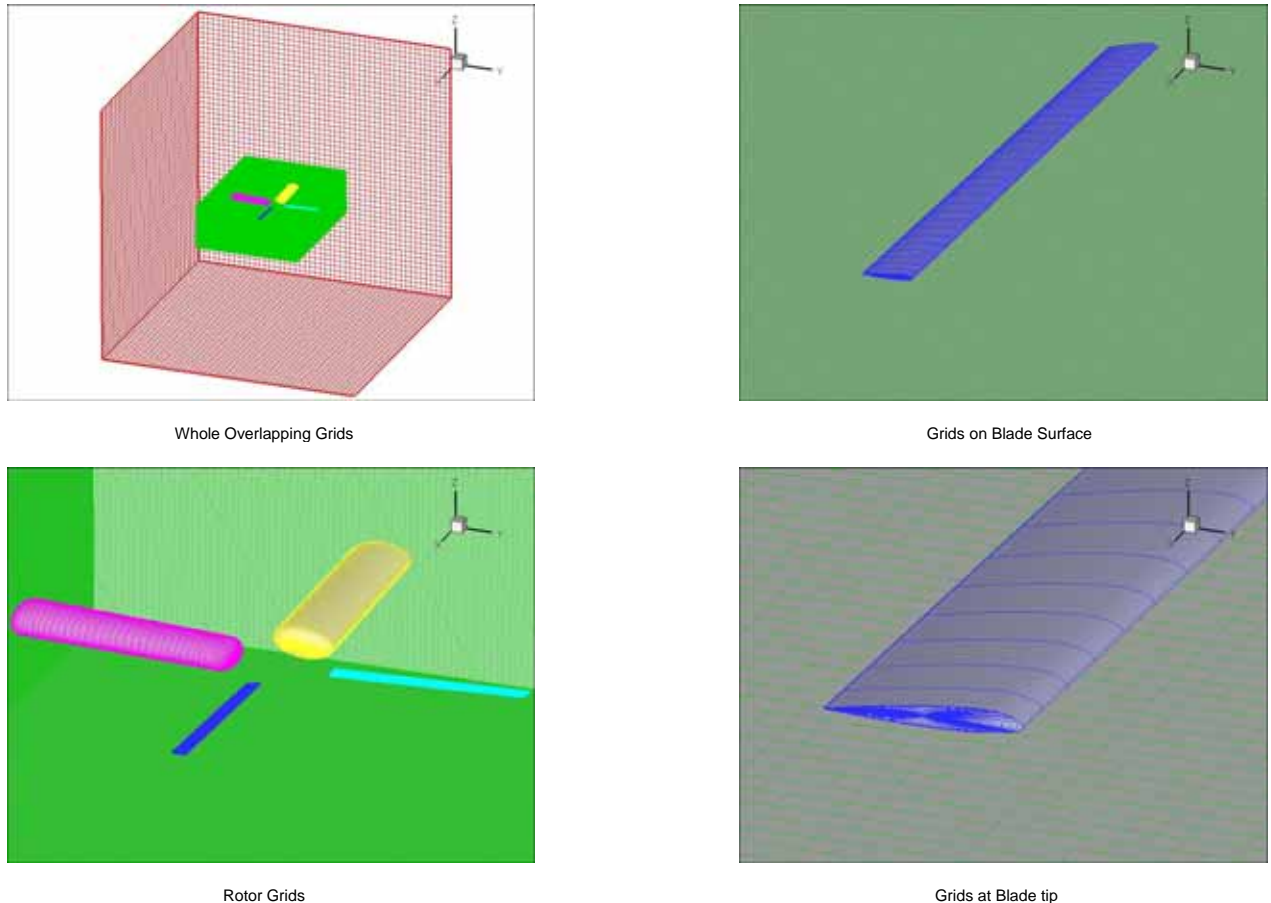


Figure 1. Overlapped grids used for this study

The outer background grid is the widest grid which is used mainly to keep the freestream condition. The upstream inflow surface is fixed to the freestream values. For other 5 surfaces, simple zero gradient extrapolation is used. The grid points of the outer background grid can be much coarser than the inner background grid.

The inner background is intended to capture the rotor wake especially the tip vortices. For this test study, a grid size of $0.15c$ is selected. However, it is insufficient to capture the BVI phenomena. In the future study, a finer inner background grid will be used.

The inner moving blade grids are constructed at each time step from a common basic blade grid. For this elastic rotor blade case, a series of axis transformations are carried out to obtain the current grid system. The elastic deformations of the blade is reflected at first, then the feathering pitch,

flapping and lead-lag, the rotor blade rotation to the corresponding azimuth angle, finally the rotor shaft tilting if any. The coordinate changes at each grid point per each time step are also calculated to obtain the time metrics. The blade motions, including the rotation, rigid motion and the elastic vibrations are reflected into the computation through the time metrics only.

Different numerical schemes are used for background grids and for the inner moving blade grids. The numerical characteristics of the computational code used at JAXA for this study are the following ones:

Moving Overlapped Grids Approach (see [16]),

Exchange information between grids at pre-designated time step,
Divided time steps for each grid to meet each maximum CFL.

Cartesian Background Grids (inner and outer),

Euler solver,
4th-order spatial accuracy, SHUS scheme (see [17]),
4-stage Runge-Kutta explicit time integration,
 $CFL \leq 0.9$ for this study.

Moving blade grids,

NS solver (use Euler only at this study),
2nd-order spatial accuracy, Harten & Yee's TVD scheme (see [18]),
Implicit time integration, 1-stage, 2nd-order conservative form,
 $CFL \leq 20$ for this study.

In the overlapped grids approach, a global time step is designated so that the rotor blade azimuth moves at a given angle increment (0.1 deg is used in this study). The allowable time step for each grid is computed according to the prescribed CFL numbers. If the global time step is smaller than or equal to the allowable time step, then the global time step is used. If the global time step is greater than the allowable time step, then the divided time step which is smaller than the allowable time step is used. The sub-time integration steps is set as $N_{\text{sub-step}} = \text{INT}(dT_{\text{global}}/dT_{\text{allowable}}) + 1$. So that $dT_{\text{sub}} = dT_{\text{global}}/N_{\text{sub-step}}$.

The flowfield information of the blade grid is interpolated onto the inner background and then onto the outer background grid at each global time step. At each sub-time integration step inside the blade grids, the background flowfield is frozen and the outer boundaries of the blade grids are interpolated from the background grid. The interpolation method used is based on the tri-linear interpolation formulation.

For this case, only one sub-time step was required for the outer and inner background grids. For the blade grids, nearly 3 steps are required. Be noticed the sub-time step number changes depending on the flowfield itself to satisfy the CFL limit.

1.2 CSD Code

The basic equations for elastic deformation of a rotor blade can be written as

Flap-wise:

$$\begin{aligned} & \left[\{EI_y + (EI_z - EI_y) \sin^2 \theta\} w'' + (EI_z - EI_y) \left(\frac{v'' \sin 2\theta}{2} + \phi v'' \cos 2\theta + \phi w'' \sin 2\theta \right) \right]'' \\ & - (Tw')' + m(\ddot{w} + e\ddot{\phi}) \\ & = F_{ax} - m(g + e\ddot{\theta} - e\Omega^2\theta) \end{aligned} \quad (1)$$

Lead-lag-wise:

$$\begin{aligned} & \left[\{EI_z + (EI_z - EI_y) \sin^2 \theta\} v'' + (EI_z - EI_y) \left(\frac{w'' \sin 2\theta}{2} - \phi v'' \sin 2\theta + \phi w'' \cos 2\theta \right) \right]'' \\ & - (Tv')' + m[\ddot{v} - e\theta\ddot{\phi} - \Omega^2(v - e\theta\phi)] \\ & = F_{ay} + m[-2\Omega\dot{u} + 2e\Omega(\dot{v}' + \theta\dot{w}') + e\theta\ddot{\theta} + \Omega^2(e_0 + 2e)] \end{aligned} \quad (2)$$

Torsion-wise:

$$\begin{aligned} & -[(GJ + Tk_A^2)\phi']' + (EI_z - EI_y) \left[(w''^2 - v''^2) \frac{\sin 2\theta}{2} + v''w'' \cos 2\theta \right] \\ & + mk^2(\ddot{\phi} + \Omega^2\phi) + me[\ddot{w} - \theta\ddot{v} + \theta\Omega^2v + e\Omega^2\phi + r\Omega^2(w' - \theta v')] \\ & = M_{ax} - m[eg + k^2(\ddot{\theta} + \Omega^2\theta + 2\Omega\theta\dot{v}')] + e\theta(e_0\Omega^2 - 2\Omega\dot{u}) \end{aligned} \quad (3)$$

Holzer-Myklestad method is used to compute the natural modes. For HART II blade, the natural modes frequencies obtained are shown in Table 1. The mode shapes are shown in Figure 2.

Table 1 Natural mode frequencies for HART II

Mode Number	Natural Mode Frequency (/rev)			
	Umarc	Boyd et al	HARTII	Present Method
1(Lag)	0.787	0.786	0.782	0.754
2(Flap)	1.11	1.111	1.125	1.138
3(Torsion)				2.66
3(Flap)			2.835	
3(Flap/Torsion)	2.8	2.8		
4(Torsion)	4.06	4.43	3.845	3.82
5(Torsion)	4.607	4.604		4.366
5(Lead-lag)			4.592	
6(Lead-lag)				4.697
6(Flap)	5.058	5.03	5.168	
7(Flap)	7.794	7.806		6.665
8(Flap)	11.171	11.199		9.237
9(Lead-lag)				11.056
10(Torsion)				11.603

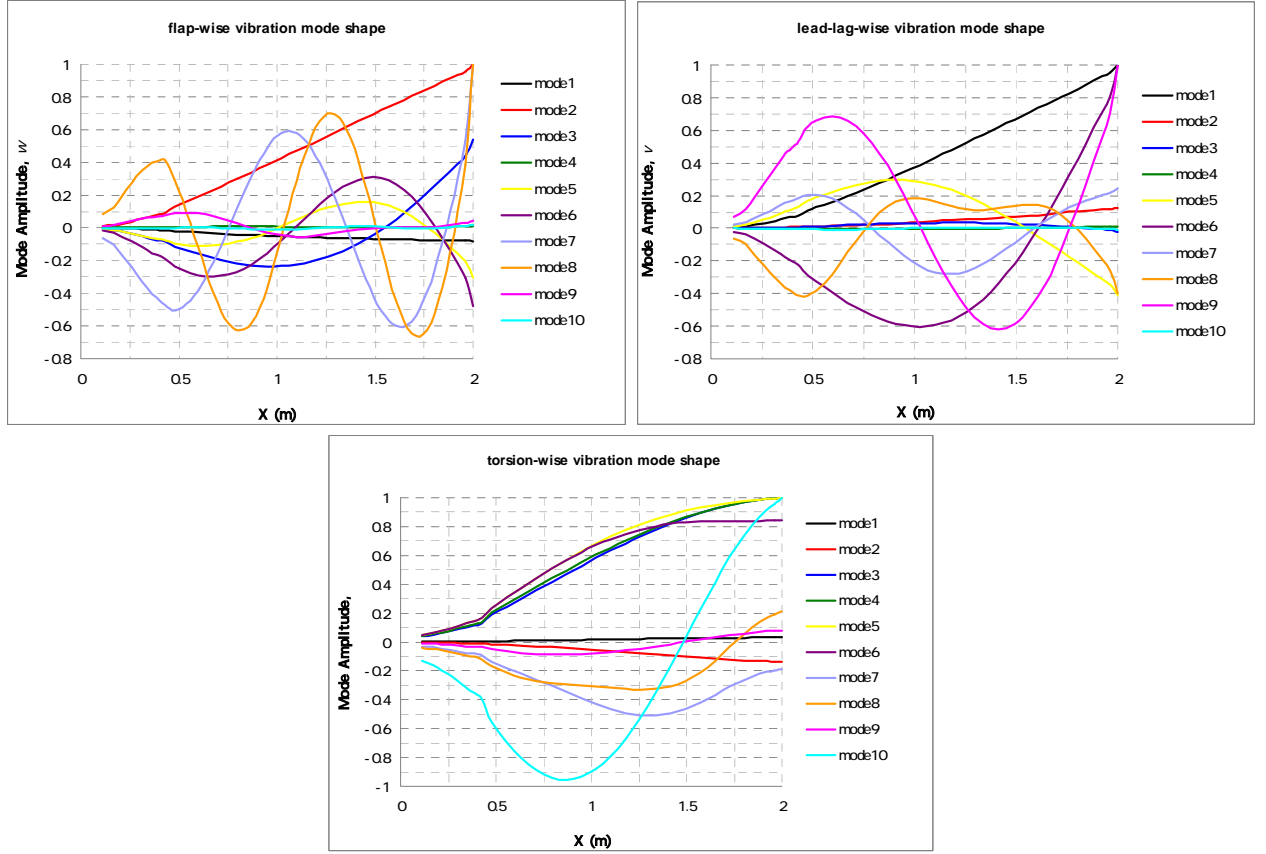


Figure 2 Natural modes for HART II blade

Mode decomposition method is used, so that the flap w , lead-lag v , and torsion angle ϕ are

$$w = \sum_{j=1}^{\infty} \bar{w}_j \cdot q_j \quad v = \sum_{j=1}^{\infty} \bar{v}_j \cdot q_j \quad \phi = \sum_{j=1}^{\infty} \bar{\phi}_j \cdot q_j \quad (4)$$

Rayleigh-Ritz approach is used to obtain the generalized equations

$$M_j \left\{ \frac{d^2 q_i}{dt^2} + \omega_j^2 \cdot q_j \right\} = Q_j \quad (j=1,2,3 \dots) \quad (5)$$

Where

$$M_j = \int_0^R \left[(k^2 \bar{\phi}_j + e \bar{w}_j - e \theta \bar{v}_j) \bar{\phi}_j + (w_j + e \bar{\phi}_j) \bar{w}_j + (\bar{v}_j - e \theta \bar{\phi}_j) \bar{v}_j \right] m dr \quad (6)$$

$$Q_j = \int_0^R \left[\{ M_{ax} - m[eg + k^2(\ddot{\theta} + \Omega^2 \theta + 2\Omega \theta \dot{v}') + e\theta(e_0 \Omega^2 - 2\Omega \dot{u})] \} \bar{\phi}_j \right. \\ \left. + \{ F_{az} - m(g + e\ddot{\theta} - e\Omega^2 \theta) \} \bar{w}_j \right. \\ \left. + \{ F_{ay} + m[-2\Omega \dot{u} + 2e\Omega(\dot{v}' + \theta \dot{w}') + e\theta \ddot{\theta} + \Omega^2(e_0 + 2e)] \} \bar{v}_j \right] dr \quad (7)$$

When there is precone angle of β_0 at the rotor hub and/or offset e_{EA} of the elastic axis with the quarter chord line (the blade axis), following substitutions in equation (7) will be required:

$$F_{az} \Rightarrow F_{az} - mr\Omega^2 \cos \beta_0 \sin \beta_0$$

$$M_{ax} \Rightarrow M_{ax} - F_{az} e_{EA} - e_{CG} mr\Omega^2 \cos \beta_0 \sin \beta_0$$

To obtain a periodic solution for equation (5) per rotor revolution as required in the loose CFD/CSD coupling approach, the 2nd time derivative of q_j is written as

$$\frac{d^2 q_j}{dt^2} = \Omega^2 \frac{d^2 q_j}{d\Psi^2} \quad (8)$$

The 2nd azimuth-wise derivative is then approximated with a central difference expression,

$$\frac{d^2 q_j}{d\Psi^2} = \frac{q_{j,i+1} - 2q_{j,i} + q_{j,i-1}}{\Delta\Psi^2} \quad (9)$$

So by solving a cyclic tri-diagonal matrix system

$$\mathbf{Ax} = \mathbf{d}$$

$$\mathbf{A} = \begin{bmatrix} b_1 & c_1 & 0\dots & a_1 \\ a_2 & b_2 & c_2 & 0\dots \\ 0\dots & \dots & \dots & \dots \\ c_N & 0\dots & a_N & b_N \end{bmatrix}, \mathbf{x} = \begin{bmatrix} q_{j,1} \\ q_{j,2} \\ \dots \\ q_{j,N} \end{bmatrix}, \mathbf{d} = \begin{bmatrix} d_1 \\ d_2 \\ \dots \\ d_N \end{bmatrix} \quad (10)$$

$$a_i = 1, b_i = \Delta\Psi^2 p_j^2 - 2, c_i = 1$$

$$d_i = \Delta\Psi^2 \Xi_{j,i}$$

the generalized amplitudes for each natural modes can be obtained without time-marching solutions. Up to 10 modes are used in present study to obtain the approximate deformations from equation (4).

1.3 Loose Coupling Approach

In the loose coupling CFD/CSD approach, periodicity of the structural deformations is assumed and the solution procedure as shown in equation (10) can be used. The CFD based aerodynamic forces and moments are saved into a CFD to CSD data file per designated azimuth angles. In this study, every 10 degrees forces data are saved and after a longer than 360/NBLD rotation, an updated CFD-based forces distribution over whole revolution can be obtained. To eliminate the initial aerodynamic disturbance just after the new trim and blade deformations are applied, half revolution CFD computation is carried out before each loose CFD/CSD iteration.

The loose CFD/CSD approach in present study is essentially same to the so-called delta methodology as proposed by AFDD [10] shown in figure 3. But it is drastically simplified by following assumptions so that the CSD code is compact enough to be directly integrated into the JAXA_ov3d CFD code.

- (1) In the CSD trim adjustment computation, only the direct control changes are taken into account for the aerodynamic forces.
- (2) Uniform inflow is assumed and based on the target trim thrust only, so it is constant during the whole computation.

Through above assumption combined with periodic deformation solution with equation (10), a simple and efficient integrated loose CFD/CSD approach is constructed. After the trim adjustment computation converges, the forces used in the CSD routines will be solely from the CFD results.

Trim adjustment is made by solve following equations:

$$\begin{bmatrix} \Delta\theta_0 \\ \Delta\theta_c \\ \Delta\theta_s \end{bmatrix} = \begin{bmatrix} \frac{\partial T}{\partial\theta_0} & \frac{\partial T}{\partial\theta_c} & \frac{\partial T}{\partial\theta_s} \\ \frac{\partial M_x}{\partial\theta_0} & \frac{\partial M_x}{\partial\theta_c} & \frac{\partial M_x}{\partial\theta_s} \\ \frac{\partial M_y}{\partial\theta_0} & \frac{\partial M_y}{\partial\theta_c} & \frac{\partial M_y}{\partial\theta_s} \end{bmatrix}^{-1} \begin{bmatrix} \Delta T \\ \Delta M_x \\ \Delta M_y \end{bmatrix} \quad (11)$$

Where

$$\begin{aligned} \Delta T &= T_{TARGET} - (T_{CFD} + T_{BET} - T_{BET,0}) \\ \Delta M_x &= M_{xTARGET} - (M_{xCFD} + M_{xBET} - M_{xBET,0}) \\ \Delta M_y &= M_{yTARGET} - (M_{yCFD} + M_{yBET} - M_{yBET,0}) \end{aligned} \quad (12)$$

The derivatives in equation (11) is estimated at each iteration numerically.

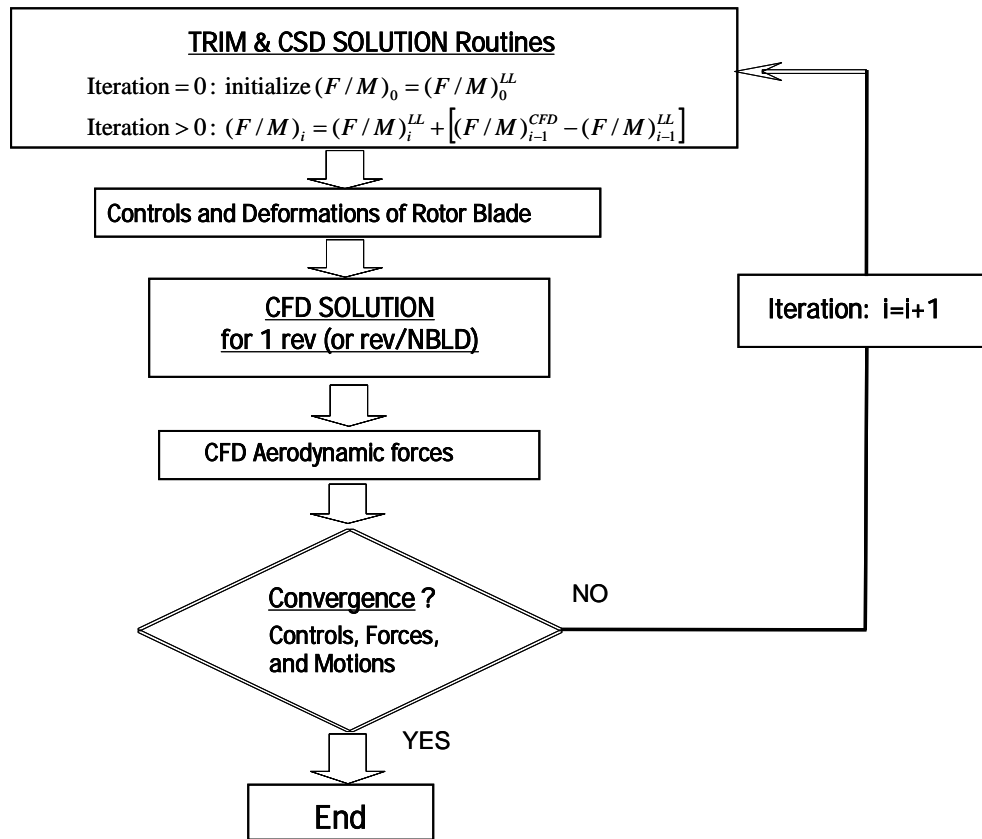


Figure 3 Loose coupling algorithm

2. COMPUTATIONAL CONDITIONS

2.1 HART II Baseline Case

HART II baseline case [19] is used for the test validation computation. The trim thrust is 3300N, which gives $C_T=0.004574$ and $C_T/\sigma=0.059375$. The trim rolling moment is 20Nm and the pitching moment is -20Nm. The corrected rotor shaft angle of 4.5 degrees is used.

2.2 Computational Grids and Boundary Conditions

The used computational grids are shown in figure 1. The blade grids are in SOH type. There is a singular line where the i-direction grids collapse into one grid at the blade tip end. The tip rectangular shape is kept in the grid system. The j-direction grids are in O-type and periodic boundary conditions are used in this direction. Although the computational cost may be a little higher when the periodic conditions are used, there are no algebraic averages at the $j=1$ (Jmax) cut surface which might introduce extra artificial diffusions. The k-direction is the off-body-wise and $k=1$ surface coincident with the blade surface.

The values at boundaries of the inner background grid are interpolated from the outer background grid. For the outer background grid, the values at the inflow surface are fixed to the free stream values. For other 5 boundaries, simple zero-th order extrapolations are used which allow mass outflow or inflow at these boundaries. For easy application of boundary conditions, the 4th order spatial accurate SHUS scheme is reduced to 2nd order MUSCL scheme at the adjacent boundaries.

2.3 Computation Settings

The CFD/CSD loose coupling iteration interval was set to 180 degrees. The CSD time increment is corresponding to 10 degrees azimuth angles.

For CFD time advancing, global time step was chosen to equivalent to 0.1 degrees azimuth angle. The CFL numbers used for background grids was 0.9 and 20 for blade grids.

3. RESULTS AND DISCUSSION

3.1 Trim Adjust History

The control adjustment history for trim at each iteration is shown in figure 4. Collective pitch angle θ_0 converges to the value that agrees with the experiment quite well. The lateral control θ_{1c} is about 1.2 degree greater than the experiment. The longitudinal cyclic control angle is about 0.5 degree higher than the experiment.

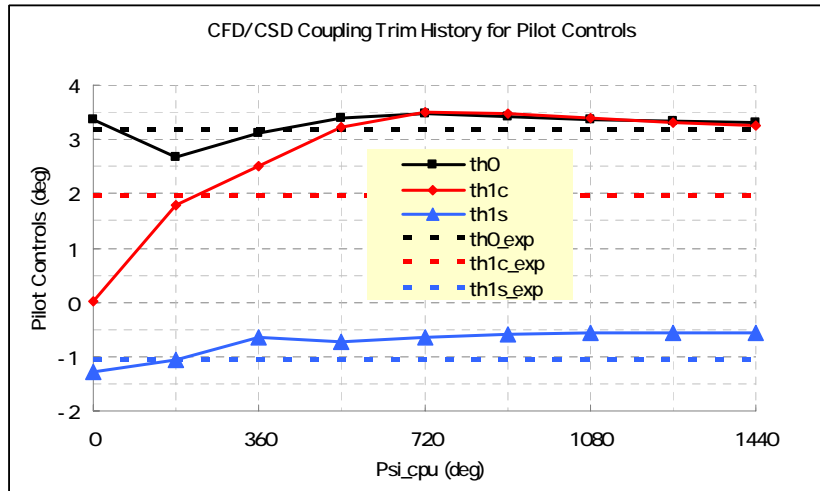


Figure 4 Trim Control Adjustment History

The CT change history is shown in figure 5. It can be seen that after 3 revolution (6 iterations), the CT is almost converges into nearly same trajectory around the target CT (experimental) value.

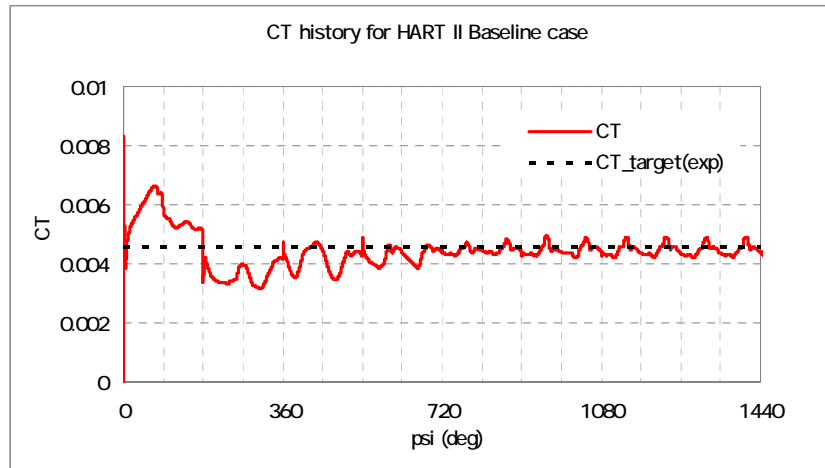


Figure 5 C_T History

3.2 Elastic Deformations

The flap motions at the blade tip for each iteration are shown in figure 6. The trajectories for the last three iterations are nearly the same which indicates the loose coupling process is almost converged. Although the total shape and vibration magnitude seems agree with the measurement, the detailed trajectory agreement is not good and mainly differs at three points, i.e., the lowest value for experiment is around 90 degrees, but the computed value is at about 65 degrees; the highest peak for experiments is at about 280 degrees, but the computation shows a peak at 230 degrees; and mostly important, around 180 degrees, there is a flap downward in computation but the experiment shows a slight rise and smooth transition from lowest value to highest value. As will be shown later, combined with the extra torsional oscillation around this position (figure 8), the $C_n M_2$ (figure 10) has a high rise peak at 180 degrees azimuth angle with is not observed in the measurement.

The lag motion (figure 7) shape agrees with the experiment very well except there is a offset. Considering the solver used is Euler, the viscous effects are not taken in account, this difference seems quite reasonable. This will be confirmed by future computations with the NS solver.

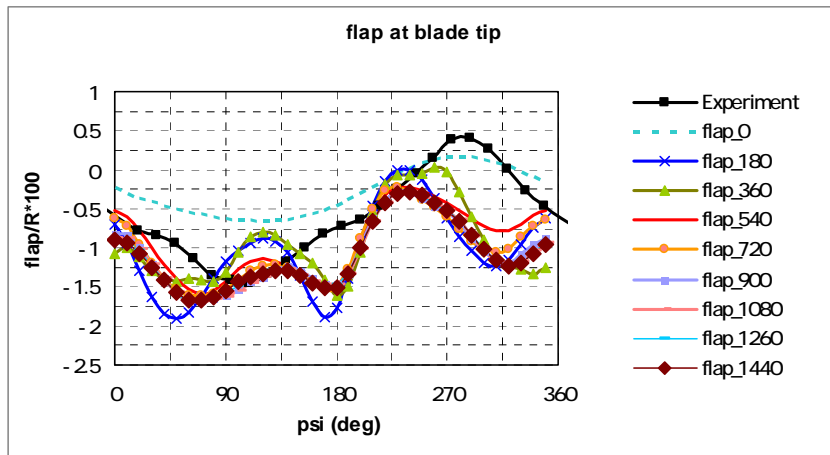


Figure 6 Flap at Blade Tip History for Iterations

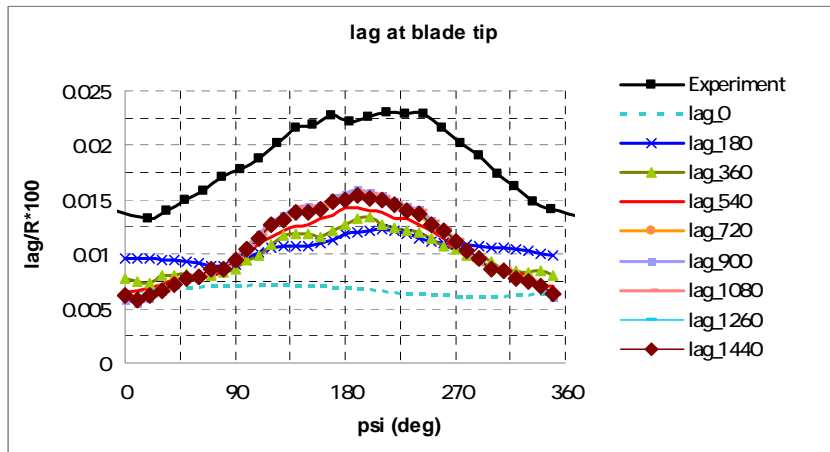


Figure 7 Lag at Blade Tip History for Iterations

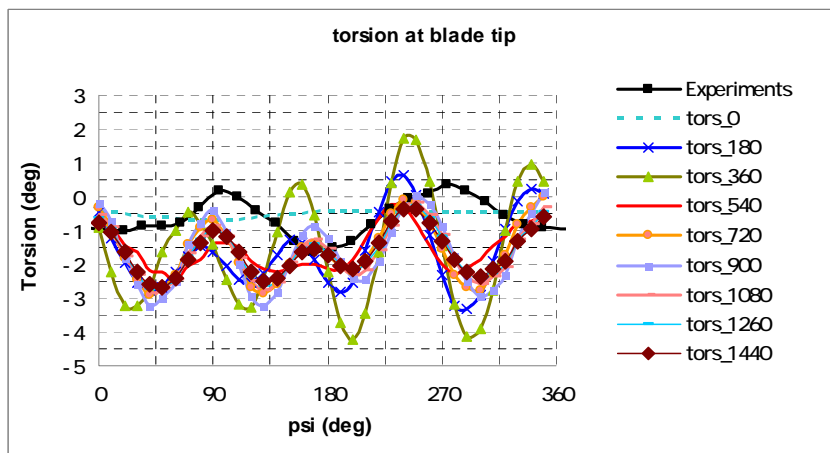


Figure 8 Torsion at Blade Tip History for Iterations

3.3 Aerodynamic Loading

As mentioned above, the CnM2 trajectory (figure 9) differs from the experiment at the 180 degree position where there is a high peak in the computation but not seen in the experiments. It is caused by flapping down combined with torsion up. Also, the BVI events are not well captured. Increasing the inner background grid resolution to preserve the tip vortices wake is necessary to improve. Anyway, the average of the computed CnM2 is nearly the same as the experiment.

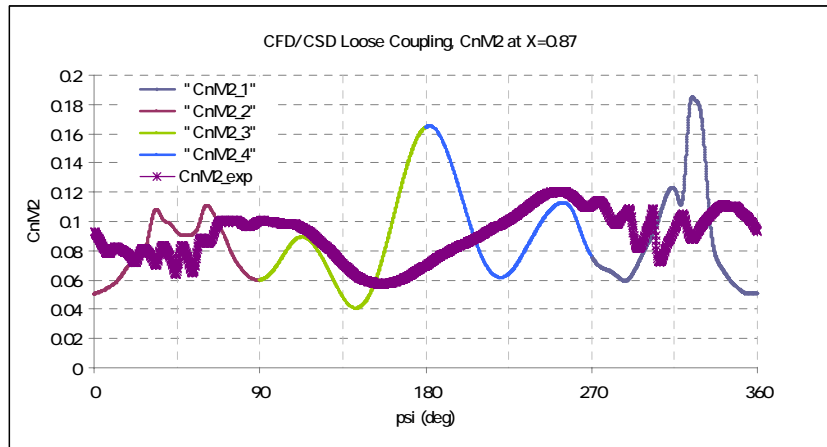


Figure 9 CnM2 at X=0.87 Comparison with Experiment

3.4 Flowfield

The iso-vorticity surface pattern is shown in figure 10. The vortex cores inside the rotor plane are hardly seen. It seems that background grid resolution is not enough to preserve the tip vortices.

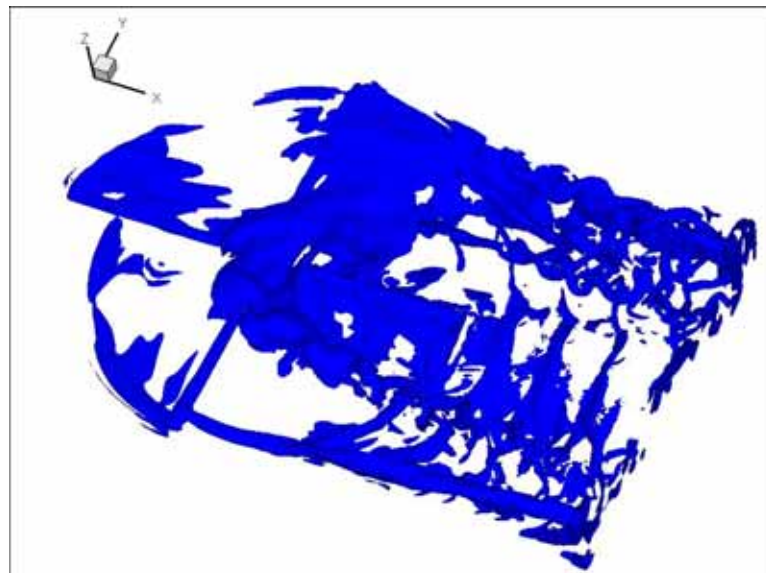


Figure 10 Iso-vorticity surface plot of the rotor wake

The rotational component of a vortex can be separated from the shear component with the so-called Q-criterion which is defined as

$$Q = -\frac{1}{2} \left[\left(\frac{\partial u}{\partial x} \right)^2 + \left(\frac{\partial v}{\partial x} \right)^2 + \left(\frac{\partial w}{\partial x} \right)^2 + 2 \left(\frac{\partial u}{\partial y} \frac{\partial v}{\partial x} + \frac{\partial u}{\partial z} \frac{\partial w}{\partial x} + \frac{\partial v}{\partial z} \frac{\partial w}{\partial y} \right) \right] \quad (13)$$

An iso-Q criterion is shown in figure 11. The tip vortices are comparably well seen. The disturbances from the root cut vortices are significant which may cause unrealistic oscillations in the aerodynamic loading.

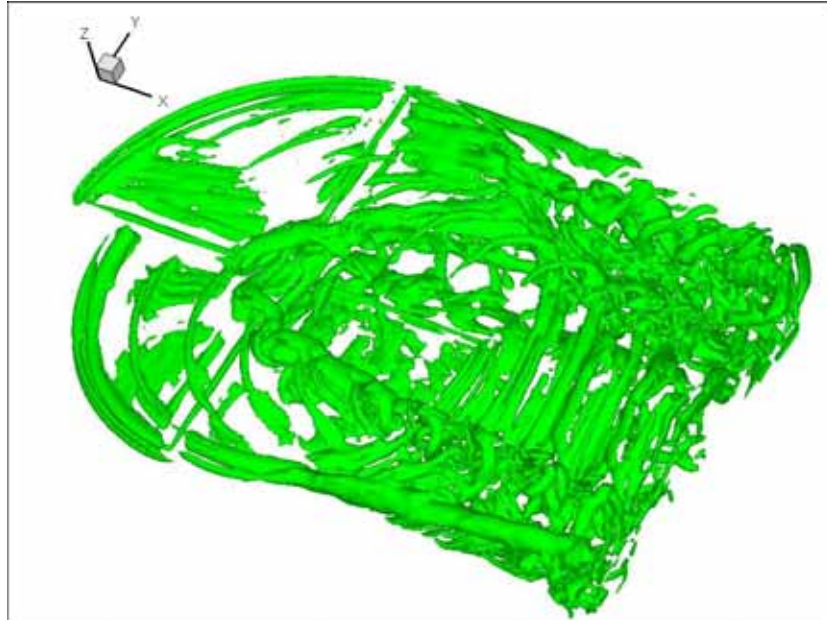


Figure 11 Iso-Q criterion plot of the rotor wake

4. CONCLUSIONS

An integrated CFD/CSD loose coupling analytical code has been developed in JAXA. The coupling approach is simplified and the comprehensive code is not required.

Test validation computation was carried out using the HART II baseline database. The trim adjustment, total thrust and the elastic motions converges very fast and stably.

The lagwise deformation of the blade show nearly the same shape of the experiment but has offset. Viscous drags neglected in current computation may be the cause of this offset.

The flapwise and torsionwise deformations of the blade shows nearly same magnitude with experiments but the shape after the trim nearly converged still remains quite different from the experiment.

The CnM2 have nearly the same average value as the experiment but the detailed shape has several differences. Especially, there is a peak around 180 degrees azimuth angle but not observed in the experiment. It is mainly caused by the elastic flap and torsion motion around this azimuth angle while the experimental result is different. Also, the detailed BVI events are not well captured. More grid points in the inner background grid may be required to preserve the tip vortices wake for good capturing of the BVI phenomena.

Further efforts will be made to improve the accuracies of the predictions. The viscous effects will be included, while the natural mode frequencies and shapes, effect of artificial structural damping, change of the loose coupling interval, etc, will be re-examined.

ACKNOWLEDGEMENT

The authors wish to thank the HART II team for their help and for the data and valuable insights. Authors would like to thank Dr.-Ing., M.S. Berend G. van der Wall for his kind support of HART II data, and Dr. Casey Burly and Dr. Chee Tung for their suggestion to participate in the HART II workshop and valuable discussion about the HART II data.

REFERENCES

- [1] C. Kitaplioglu, F.X. Caradonna, and C.L. Burley, "*Parallel Blade-Vortex Interactions: An Experimental Study and Comparison with Computations,*" Journal of the American Helicopter Society, pp.272-281, July (1997).
- [2] C. Kitaplioglu, F.X. Caradonna, and M. McClur, "*An Experimental Study of Parallel Blade-Vortex Interaction Aerodynamics and Acoustics Utilizing and Independently Generated Vortex,*" NASA/TM-1999-208790, July (1999).
- [3] Sooga Lee and Daniel Bershader, "*Head-On Parallel Blade-Vortex Interaction,*" AIAA Paper No,91-3277, 9th Appliel Aerodynamics Conference, Baltimore, MD, Sept. 23-26, (1991).
- [4] Duck-Joo Lee, Chi-Hoon Cho, Yung H.Yu, "*Simulation of BVI noise generation using Computational Aeroacoustics,*" INTER-NOISE 2006, Honolulu, Hawaii, USA, 3-6 December, (2006).
- [5] Y. Tanabe, S. Saito, K. Takasaki, and H. Fujita, "*A parametric study on parallel Blade-Vortex-Interaction Noise,*" INTER-NOISE 2007, Istanbul, Turkey, 28-31 August 2007.
- [6] C. Benoit, J.-O. Gretay, G. Jeanfaivre, S. Peron, J. Sides; Y. Tanabe, S. Saito, C. Yang, and T. Aoyama, "*Inviscid numerical simulations of 2D parallel blade-vortex interaction,*" ONERA Technical Report, No. RT 1/11474 DSNA, March 2007.
- [7] N. Kobiki, N. Kondo, S. Saito, T. Akasaka, and Y. Tanabe, "*Active Tab, a New Active Technique for Helicopter Noise Reduction,*" 29th European Rotorcraft Forum, 2003.
- [8] Altmikus, A.R.M., Wagner, S., Beaumier, P., and Servera, G., A comparison, "*Weak versus Strong Modular Coupling for Trimmed Aeroelastic Rotor simulations,*" American Helicopter Society 58th Annual Forum, Montreal, Quebec, June, 2002.
- [9] Potsdam, M., Yeo, H., Johnson, W., "Rotor Airloads prediction Using Loose Airodynamic / Structural Coupling," 60th American Helicopter Society Annual Forum, Baltimore, MD, 2004.
- [10] J.W. Lim, T.A. Nygaard, R. Strawn, and M. Potsdam, "BVI airloads prediction using CFD/CSD Loose Coupling," American Helicopter Society Fourth Vertical Lift Aircraft Design Conference, San Francisco, CA, January 2006.
- [11] M. J. Hill, "*Coupled fluid-structure simulations of helicopter rotors,*" Thesis, Department of Aerospace Engineering, The Graduate School, The Pennsylvania State University, August 2006.
- [12] B.W. Sim and J.W. Lim, "*Blade-vortex interaction (BVI) noise & airload prediction using loose aerodynamic/structural coupling,*" American Helicopter Society 62nd Annual Forum, Phoenix, Arizona, May 2006.
- [13] K. Noboru, S. Saito, T. Fukami, T. Komura, "*Design and Performance Evaluation of Full Scale On-board Active Flap System,*" American Helicopter Society 63rd Annual Forum, Virginia Beach, VA, May 1-3, 2007.

- [14] S. Saito, Y. Tanabe, A. Hashimoto, Y. Nakamura, Y. Choongmo, T. Aoyama, “*Aeroelastic simulation of HART II model using moving overlapped grid approach*,” 32nd European Rotcraft Forum, Netherland, 2006.
- [15] Y. Tanabe, S. Saito, Y. Choongmo, T. Aoyama, A. Hashimoto, Y. Nakamura, “*Aeroacoustic and Aeroelastic Simulation of HART II Model Rotor With Moving Overlapped Grid Approach*,” INTER-NOISE 2006, Hawaii, 2006.
- [16] A. Ochi, T. Aoyama, S. Saito, E. Shima, and E. Yamakawa, “*BVI Noise Predictions by Moving Overlapped Grid Method*,” AHS 55th Annual Forum, May 1999.
- [17] E. Shima and T. Jounouchi, “*Role of CFD in Aeronautical Engineering (No.14) - AUSM Type Upwind Schemes -*,” NAL SP-34, 1999, pp.7-12.
- [18] H.C. Yee and A. Harten, Implicit TVD Schemes for Hyperbolic Conservation Laws in Curvilinear Coordinates, AIAA Journal, Vol. 25, No.2, February 1987, pp.266-274.
- [19] Y.H. Yu, C. Tung, B. van der Wall, H.-J. Pausder, C. Burley, T. Brooks, P. Beaumier, Y. Delrieux, E. Mercker, and K. Pengel, “*The HART-II Test: Rotor Wakes and Aeroacoustics with Higher-Harmonic Pitch Control (HHC) Inputs - The Joint German/French/Dutch/US Project -*,” AHS 58th Annual Forum, Montreal, Canada, June 11-13, 2002.